

# UBVI CCD Photometry of Berkeley 55 Open Cluster

İnci Akkaya Oralhan<sup>1,\*</sup>

<sup>1</sup>Department of Astronomy and Space Sciences, Science Faculty, Erciyes University, TR-38039, Kayseri, Turkey.  
\*Corresponding author. E-mail: iakkaya@erciyes.edu.tr

MS received 26 January 2021; accepted 26 January 2021

**Abstract.** Fundamental astrophysical parameters have been derived for Be 55 open cluster based on *UBVI* CCD photometric data, observed with the AZT-22 1.5m telescope at Maidanak Astronomical Observatory in Uzbekistan. The mean reddening is obtained as  $E(B-V)=1.77\pm 0.10$  mag from early type members. The zero age main sequence fitting in the  $Q_{V\lambda}-Q'$  diagrams indicates the distance modulus,  $(V_0-M_V)=12.4\pm 0.20$  mag ( $d=3.02\pm 0.28$  kpc). This photometric distance is consistent with the distances of Gaia EDR3 ( $d=3.09\pm 0.16$  kpc) and period-luminosity relation ( $d=2.78\pm 0.32$  kpc) of its Cepheid *S5* within the uncertainties. This distance also locates the cluster near the Perseus spiral arm. The Geneva isochrone fittings to the Hertzsprung-Russell diagram and observational colour-magnitude diagrams derive turn-off age,  $85\pm 13$  Myr, by taking care five red supergiants/bright giants. The possible inconsistencies on the locations of the bright giants with the rotating/non-rotating isochrones may be due to both the age spread of stars in young open clusters and the diversity in rotational velocities.

**Keywords.** open clusters and associations: individual Berkeley 55- stars: early-type stars- evolution: late-type supergiants

## 1. Introduction

Be 55 was studied by Negueruela & Marco (2012) (hereafter N12), Lohr et al. (2018) (hereafter L18), and Alonso-Santiago et al. (2020) (hereafter A20). N12 identified populations of B-type stars, one F-type and four late-type red supergiants/bright giants (RSGs/RBGs), two Blue Stragglers (BS). Their spectroscopic and photometric analyses indicated an age of  $50\pm 10$  Myr and a distance of  $d\approx 4$  kpc. Its member *S5* was identified by L18 as a Type I Cepheid with a pulsation period 5.85 day. Spectral types, effective temperatures and radial velocities of these bright giants have been obtained by A20 from the medium-resolution spectroscopic observations of the 4.2 m William Herschel Telescope at La Palma. They updated the distance and age of Be 55 as  $3.24\pm 0.22$  kpc and  $63\pm 15$  Myr, respectively from PARSEC isochrones (Bressan et al., 2012). Be 55 were also studied by Maciejewski & Niedzielski (2007), Tadross (2008), Bukowiecki et al. (2011), and Molina Lera et al. (2018), respectively (See Table 7).

As emphasized by A20, Cepheids in young open clusters (OCs) which lie on the blue loop as pulsating variable, have great importance for distance estimation. For their distances, there are useful period-luminosity relations (PLR) in the literature (Benedict et al. , 2007; Anderson et al. , 2013; Lazovik and Ras-

torguev , 2020). Some young OCs with Cepheids as an example are as the following, van den Bergh-Hagen (Marco et al., 2014), Be 51 (Negueruela et al., 2018), NGC 6649 and NGC 6664 (Alonso-Santiago et al. , 2020).

Young OCs are generally heavily obscured. For their reddenings,  $Q$  technique from their early-type stars is used (Sung et al., 2013) (hereafter S13). For their bright evolved stars, the intrinsic colours of Fernie (1963) and Fitzgerald (1970) for (UBV) and Koornneef (1983) for JHK<sub>s</sub> are utilised.

In this paper new Maidanak *UBVI* CCD Photometry of Be 55 is presented, and analysed by utilising Gaia EDR3 astrometric/photometric data (Brown et al. , 2020; Lindegren et al. , 2020). The issues mentioned above have been studied. As emphasized by Lindegren et al. (2020), compared to Gaia DR2 (Brown et al. , 2018; Lindegren et al. , 2018), the average improvement on the uncertainties of parallax/proper motion data of Gaia EDR3 is almost a factor 0.8 for the parallaxes, and 0.5 for the proper motions.

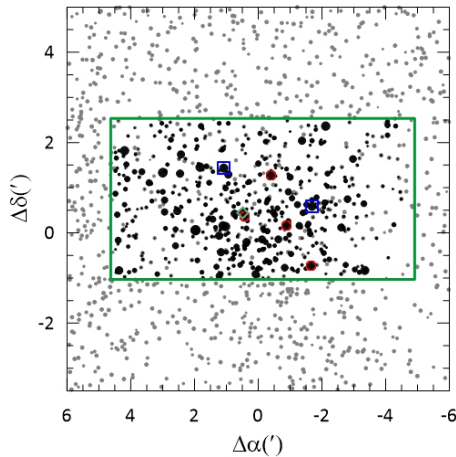
This paper is organized as follows: Section 2 describes the observation and data reduction. The radius, membership selection, the determination of the reddening, and distance modulus/distance are presented in Section 3. Be 55's age plus kinematics/orbital parameters of its bright giants are given in Sections 4–5. A Discussion and Conclusion is presented in Section 6.

**Table 1.** For *UBVI* filters, exposure time, *FWHM*-seeing, the primary/secondary extinction coefficients ( $k_{1\lambda}$ ,  $k_{2\lambda}$ ), and the photometric zero-point ( $\zeta_\lambda$ ).

Filter	Colour	Exposure time (s)	<i>FWHM</i> -seeing (")	$k_{1\lambda}$	$k_{2\lambda}$	$\zeta_\lambda$
U	U-B	600	1.22	0.423±0.022	0.023	21.560±0.011
B	B-V	20, 600	1.99	0.324±0.010	0.026	23.261±0.006
V	B-V	10, 300	0.88	0.231±0.009	-	23.396±0.001
I	V-I	10, 120	0.74	0.139±0.010	-	23.017±0.009

**Table 2.** Photometric data of Be 55.

$\alpha_{2000}$ (h m s)	$\delta_{2000}$ (° ' ")	V- mag	( <i>U</i> - <i>B</i> )	( <i>B</i> - <i>V</i> )	( <i>V</i> - <i>I</i> )	eV	e( <i>V</i> - <i>I</i> )	e( <i>B</i> - <i>V</i> )	e( <i>U</i> - <i>B</i> )
21 16 51.27	51 46 07.3	15.186	0.524	1.562	2.130	0.003	0.011	0.004	0.009
21 17 2.30	51 46 58.1	14.666	0.581	1.543	2.017	0.001	0.001	0.001	0.006
21 17 1.72	51 46 49.1	15.771	0.721	1.532	2.021	0.001	0.005	0.004	0.016
...	...	...	...	...	...	...	...	...	...
...	...	...	...	...	...	...	...	...	...
...	...	...	...	...	...	...	...	...	...

**Figure 1.** The star chart of Be 55 based on Gaia EDR3 data (grey dots) and Maidanak 2k data (black dots). The position of the stars is relative to its mean equatorial coordinates. Green rectangular shows the field of view of Maidanak detector. Five RSGs/RBGs and two BSs are also indicated (see Fig. 6 for the symbols).

## 2. Observation and Data Reduction

The observation in Johnson-Cousins' *UBVI* system of Be 55 was carried out with the AZT-22 1.5-m (*f*/7.74) Ritchey-Chretien telescope at Maidanak Astronomical Observatory (MAO) in Uzbekistan, during high-quality photometric night, on 2005 August 9. Images were taken with the *SITe* 2k CCD detector, which has 2000×800 pixels, a gain of 1.16 e<sup>-</sup>/ADU and a readout noise of 5.3 e<sup>-</sup>. The combination of the telescope and the detector ensures an unveignetted field of view of 8.85' × 3.55'. Standard magnitude for a given filter  $\lambda$  is obtained using

the following relation,

$$M_\lambda = m_\lambda - [k_{1\lambda} - k_{2\lambda}C]X + \eta_\lambda C + \zeta_\lambda \quad (1)$$

where  $m_\lambda$ ,  $k_{1\lambda}$ ,  $k_{2\lambda}$ ,  $C$ , and  $X$  are the observed instrumental magnitude, primary/secondary extinction coefficients, colour index and air mass, respectively.  $M_\lambda$ ,  $\eta_\lambda$ ,  $\zeta_\lambda$  are standard magnitude, transformation coefficient and photometric zero point, respectively. The other details of data reduction can be found in Lim et al. (2009). The SAAO standard stars in Menzies et al. (1991) and Kilkenny et al. (1998) were used to derive atmospheric extinction and transformation coefficients. Pre-processing was performed using the IRAF/CCDRED package and an aperture of 10" was used for standard star photometry. Exposure time (s), *FWHM*-seeing ("), extinction coefficients and zero points for *UBVI* filters are given in Table 1. Here, *FWHM*-seeing means the seeing, which is estimated from full width at half maximum of the point like stars on the images. The photometric data of 357 stars are listed in Table 2 for a sample data.

Be 55 star chart is displayed in Fig. 1. Its mean central equatorial (J2000) and the Galactic coordinates are as the following, RA = 21<sup>h</sup> 16<sup>m</sup> 58<sup>s</sup>.01, Dec = +51° 45' 32".04;  $\ell$  = 93°.027,  $b$  = 1°.798, respectively.

The mean photometric errors of *V* mag, the colour indices (*V* - *I*), (*B* - *V*) and (*U* - *B*) against *V*-mag for Be 55 are presented in Table 3. The photometry for Be 55 is compared to the *UBV* CCD photometry of N12. For 26 common stars, the differences of  $\Delta V$  and  $\Delta(B - V)$  against (*B* - *V*), and the difference of  $\Delta(U - B)$  against (*U* - *B*) are displayed in Fig. 2. When the large deviant data of the evolved stars are excluded from the

**Table 3.** The mean photometric errors of  $\langle V \rangle$  mag,  $\langle (V - I) \rangle$ ,  $\langle (B - V) \rangle$  and  $\langle (U - B) \rangle$  against  $V$ -mag.

$V$	$\langle \sigma_V \rangle$	$\langle \sigma_{V-I} \rangle$	$\langle \sigma_{B-V} \rangle$	$\langle \sigma_{U-B} \rangle$
13-14	0.003	0.013	0.008	0.005
14-15	0.005	0.020	0.007	0.016
15-16	0.008	0.007	0.007	0.017
16-17	0.005	0.007	0.009	0.032
17-18	0.006	0.009	0.010	0.065
18-19	0.012	0.016	0.023	0.129
19-20	0.016	0.021	0.053	-
20-21	0.050	0.052	0.123	-
21-22	0.090	0.095	0.156	-
22-23	0.150	0.157	-	-

calculation, the mean differences together dispersions of  $V$  and  $(B - V)$  are  $\Delta V = +0.036 \pm 0.027$  mag and  $\Delta(B - V) = +0.003 \pm 0.012$ , respectively. The difference,  $\Delta(U - B)$  is  $+0.082 \pm 0.064$ , which is systematically bluer than N12. For the interval of  $14 < V < 18$  mag, the  $V$  magnitudes of N12 seem to be slightly fainter. For  $14 < V < 18$  mag,  $(B - V)$  values of this paper are in good consistent with N12, except for bright giants. In panel (c) there appears a discrepancy between  $-0.4$  to  $-1.0$  in  $(U - B)$  of four RBGs/RSGs between N12 and Maidanak observations. For Cepheid S5 (red diamond), the discrepancy is about  $0.50$  mag in  $\Delta V$  and  $0.2$  mag in  $\Delta(B - V)$  from panels (a) and (b). The reason for large colour difference for four late-type supergiants with very red colours between  $(U - B)$  of present photometry and N12 is due to the so-called red leak in the used  $U$  filter. Therefore, their  $U$ -magnitudes of present photometry are brighter than N12. However, there is no any red leak effect in the used  $U$  filter, as is seen from table 2 of the transformation coefficients of Lim et al. (2009).

### 3. Fundamental Parameters of Be 55

#### 3.1 Radius of Be 55

For the size of Be 55, its stellar radial density profile (RDP) (Fig. 3) is constructed from the Gaia EDR3 photometric/astrometric data for the field and cluster members within  $15'.0$ , down to  $G = 20$  mag. Its RDP has been constructed by counting stars in concentric rings of increasing width with distance to its centre. The number and width of rings were optimised so that the resulting RDP had adequate spatial resolution with moderate  $1\sigma$  Poisson errors (Bonatto and Bica, 2007). The solid curve (Fig. 3) denotes the fitted King's profile (King, 1966). The two-parameter function,  $\sigma(R) = \sigma_{bg} + \sigma_0 / (1 + (R/R_c)^2)$  is adopted. Here,  $\sigma_{bg}$  is the residual background density,  $\sigma_0$  the central density of stars, and  $R_{core}$  the core radius. The

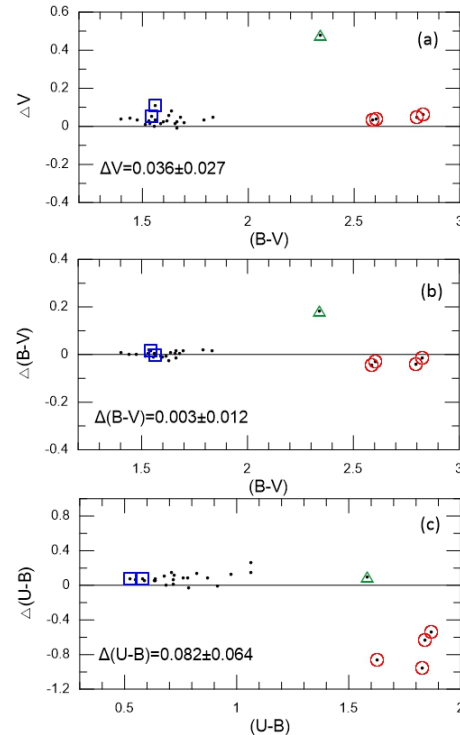


**Figure 2.** The differences of  $V$  mag,  $(B - V)$  and  $(U - B)$  as a function of  $(B - V)$  and  $(U - B)$ .  $\Delta$  means this paper - N12. Five RSGs/RBGs are plotted for just presentation (for the symbols, see Fig. 6).

horizontal gray bar shows the stellar background level measured in the comparison field. From Fig. 3, the core and cluster radii have been determined as  $(R_{core}, R_{RDP}) = (0'.45, 2'.5)$ . The cluster radius is compatible with  $2'.5$  of Molina Lera et al. (2018) and  $2'.2$  of Sampedro et al. (2017).  $R_{core}$  value of this paper is less than  $1'.32$  of Bukowiecki et al. (2011),  $0'.90$  of Kharchenko et al. (2013), and  $1'.28$  of A20, respectively.

#### 3.2 Membership Selection

As is seen in the papers of Akkaya Oralhan et al. (2019) and Akkaya Oralhan et al. (2020),  $UBVI$  photometric data of Be 55 have been combined with Gaia EDR3 proper motion and parallax data (Brown et al., 2020; Lindegren et al., 2020) to classify the likely cluster members. On the  $(\mu_\alpha, \mu_\delta)$  plane (Fig. 4), 305 stars (filled dots) within  $R_{RDP} = 2'.5$  are displayed. The grey dots represent the field background/foreground stars with a region centered around 15 arcmin. The fitted radius (red circle) by eye is determined as  $0.5 \text{ mas yr}^{-1}$  by utilising the histograms (shown with red lines) attached to the  $\mu_\alpha$  versus  $\mu_\delta$  plot. 109 probable members in the red circle are used to calculate from both the median values ( $\langle \mu_\alpha \rangle$  and  $\langle \mu_\delta \rangle$ ) and the quantity  $\mu_R = \sqrt{(\mu_\alpha - \langle \mu_\alpha \rangle)^2 + (\mu_\delta - \langle \mu_\delta \rangle)^2}$ . Parallax

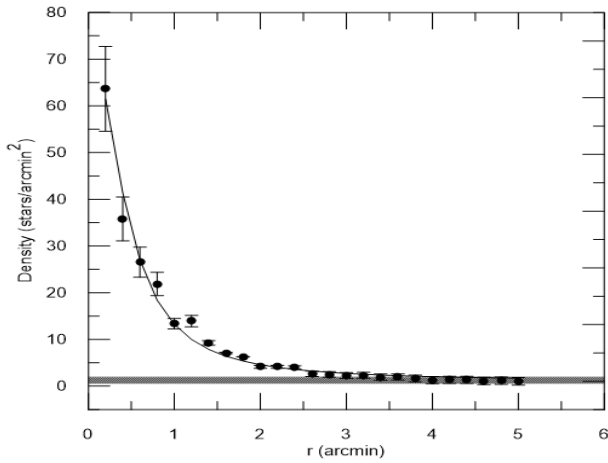


**Figure 3.** The radial density profile of Be 55. The curved line shows the fitting of King (1966). The vertical bars denote the Poisson errors.

histogram and  $(G, G_{BP} - G_{RP})$  diagram are presented in the bottom of Fig. 4. The blue and black histograms show 305 and 109 members, respectively. The number of 109 members is in good agreement with the 107 members, classified by Cantat-Gaudin et al. (2018, 2020). The applied median Gaia EDR3 parallax ( $\varpi = 0.317 \pm 0.059$  mas) on the histogram gives 64 members, and these provide a single stellar sequence (black dots) in the  $(G, G_{BP} - G_{RP})$  diagram. Since the current Gaia EDR3 parallaxes of the individual stars have a random error, the ensemble median parallax is considered. Accordingly the parallax error is the median of the members. The median astrometric values of 64 members are  $(\mu_\alpha, \mu_\delta) = (-4.070 \pm 0.078, -4.662 \pm 0.070)$  mas yr<sup>-1</sup> and  $\varpi = 0.317 \pm 0.059$  mas, respectively which are compatible with  $(\mu_\alpha, \mu_\delta) = (-4.050 \pm 0.219, -4.618 \pm 0.214)$  mas yr<sup>-1</sup> and  $\varpi = 0.309 \pm 0.091$  mas, given by Cantat-Gaudin et al. (2018, 2020).

The determination of the age of Be 55 depends on the memberships of five RSGs/RBGs and two BSs. As was done by L18 (see their figs. 7-10), to query on their memberships further, their Gaia EDR3 parallaxes against G-mag plus  $\mu_\alpha$  versus  $\mu_\delta$  are displayed in Fig. 5(a) and (b). In panel (a) the vertical lines indicate the median Gaia EDR3 parallax  $\varpi = 0.317 \pm 0.059$  mas (dashed black line), and photometric parallax  $\varpi = 0.331 \pm 0.043$  from  $Q_{V\lambda} - Q'$  (orange line, see section 3.4), respectively. As is noticed from panel (a), the parallax uncertainties of five RSGs/RBGs and two BSs (Table 5) almost remain within the error limits of the vertical/horizontal lines. Note that S6/L145's parallax value is far from the median parallax. But its uncertainty remains the error limit of horizontal dashed line. Here, the notation "L" represents the star ID in L18.

The proper motions of five RSGs/RBGs and two

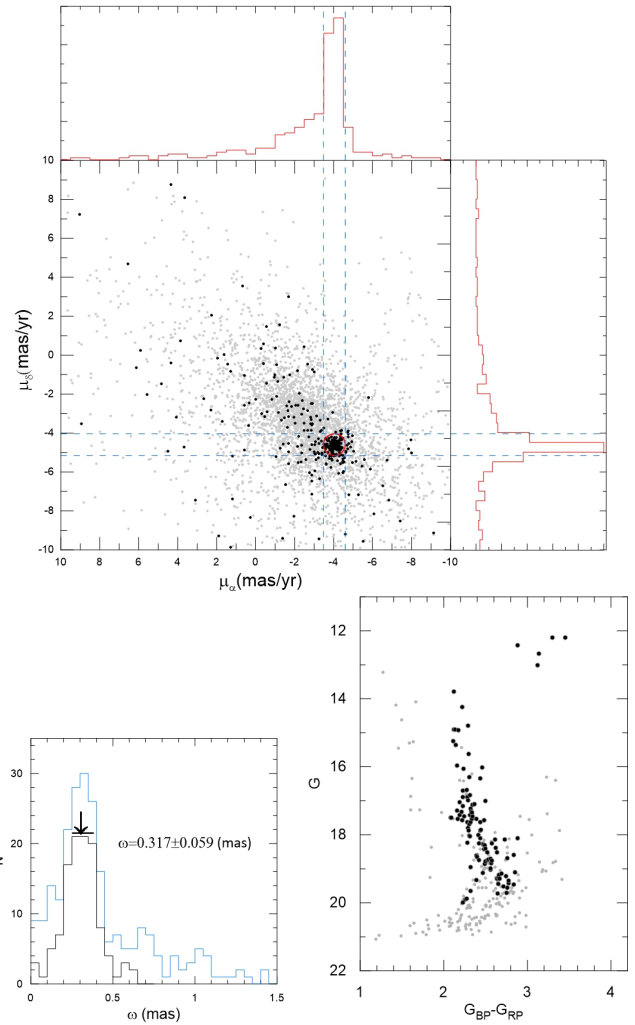


**Figure 4.** The  $\mu_\alpha$  versus  $\mu_\delta$  for 305 stars of Be 55 (filled dots). The field stars inside 15 arcmin are shown with small grey dots. There are probable 109 members in the red circle as the fitted proper motion circle (0.5 mas yr<sup>-1</sup>). Gaia EDR3 parallax ( $\varpi$ ) histogram (left panel) for 305 (blue) and 109 members (red). On  $(G, G_{BP} - G_{RP})$ , a single stellar cluster sequences of the probable members are clearly visible.

BSs together their errors are inside the borders of the blue circle (panel b). Blue circle is constructed as the following, the derivation of the relation  $V_{tan} = 4.74\mu/\varpi$  provides  $\sigma_{V(tan)} = 4.74\sigma_\mu/\varpi$ . In this case, it is assumed that the adopted  $\varpi$  has no error, and that the velocity of stars in Be 55 is homogeneous and isotropic,  $\sigma_{V(tan)} = \sigma_{V(rad)}$ . A20 give the average radial velocity of the bright giants of Be 55 as  $V_{rad} = -27.7 \pm 4.9$  km s<sup>-1</sup>. Then the expected dispersion in proper motion is obtained as  $\sigma_\mu = (4.9 \text{ kms}^{-1}) \times \varpi (= 0.317 \text{ mas}) / 4.74 = 0.33$  mas yr<sup>-1</sup>. In that case these all seem to be members, for this respect the derived age in this paper is safely interpreted. The global parallax zero point shift,  $\Delta\varpi = -0.017$  mas of Gaia EDR3 (Brown et al., 2020)

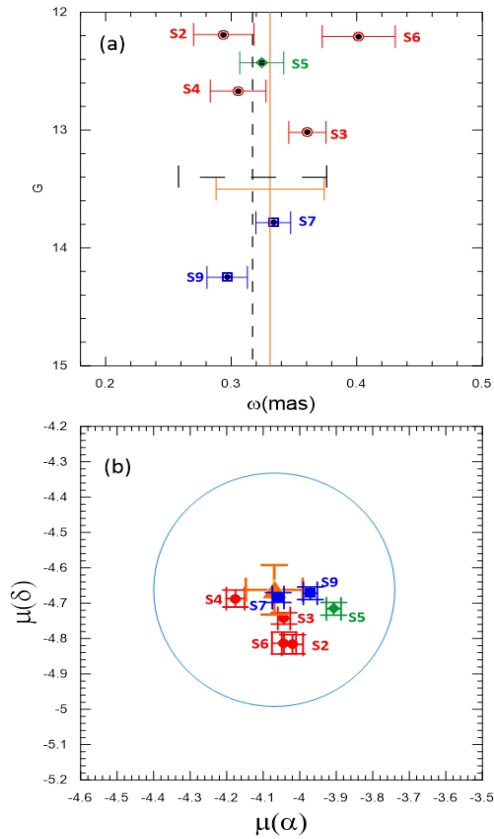


**Figure 5.** GaiaEDR3 parallax ( $\varpi$ ) against  $G$  mag (panel a) and the  $\mu_\alpha$  versus  $\mu_\delta$  (panel b) for five RSGs/RBGs and two BS candidates. The median Gaia EDR3/photometric parallaxes are shown with the vertical dashed black and solid orange lines together their uncertainties (horizontal lines), respectively. The orange triangle of panel (b) denotes the median Gaia EDR3 proper motion components of Be 55. The blue circle represents the expected dispersion ( $0.33 \text{ mas yr}^{-1}$ ) in proper motion.

is applied to the median value,  $0.317 \text{ mas}$ , it gives a close distance up to  $0.16 \text{ pc}$ .

The distribution of 64 probable members on the CMDs,  $(V, U - B)$ ,  $(V, B - V)$ , and  $(V, V - I)$  is presented in Fig. 6. Maitanak *UBVI CCD* observations of the cluster on the CMDs are shown with grey symbols; 89 (panel a), 357 (panel b), 403 (panel c), respectively. Diamond, filled red circles, and blue squares represent one Cepheid, four RSGs/RBGs and two BSs, respectively. Star designation is from N12.

### 3.3 Reddening

The reddening of Be 55 is determined from 38 early type members with  $V < 16 \text{ mag}$  and  $(U - B) < 1.1$  on the  $(U - B)$ ,  $(B - V)$  (CC) colour-colour plot (Fig. 7). Out of 64 members, 46 members have *UBV* data. Five members with a red circle are the RSGs/RBGs. The mean reddening from these early type members is estimated as  $E(B - V) = 1.77 \pm 0.10 \text{ mag}$ , and thus the red-

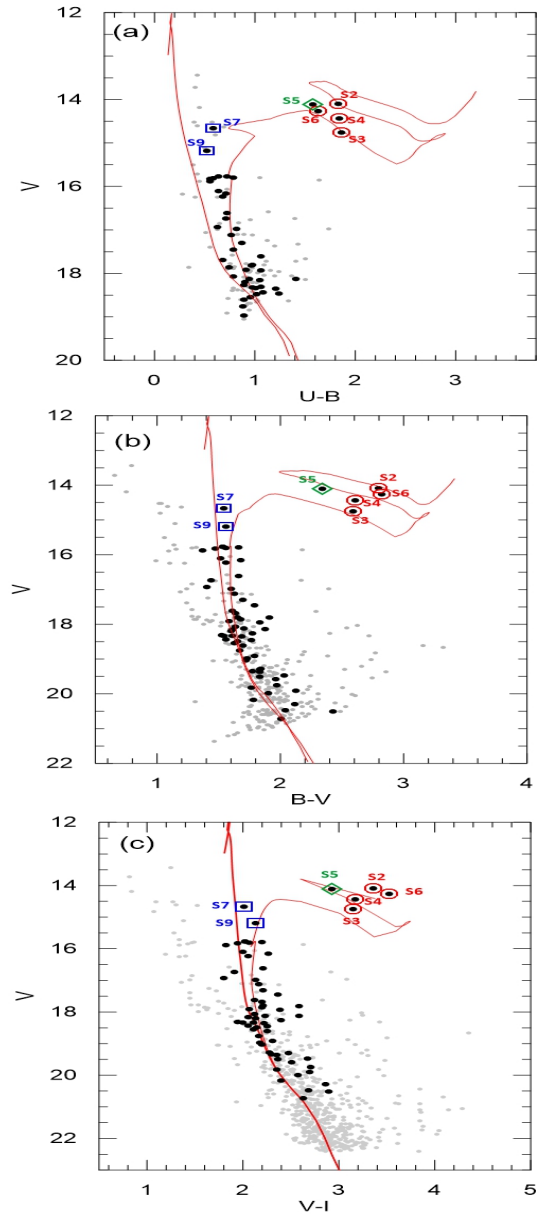


**Figure 6.** The CMDs of the members;  $V-(U - B)$  ( $N=46$ , panel a),  $V-(B - V)$  ( $N=64$ , panel b) and  $V-(V - I)$  ( $N=64$ , panel c). Solid red lines/curves denote the E12 ZAMS/85 Myr isochrones. Maitanak *UBVI CCD* observations are shown with grey symbols; 89 (panel a), 357 (panel b), 403 (panel c), respectively. Diamond, filled red circles, and blue squares represent one Cepheid, four RSGs/RBGs and two BSs, respectively. Star designation is from N12.

dened colour sequence of the Schmidt-Kaler (SK82) (Schmidt-Kaler, 1982) (red curve) is fitted to the CC diagram. For the determination of  $E(B - V)$ , the reddenings  $E(V - I)$ ,  $E(V - J)$ ,  $E(V - H)$ , and  $E(V - K_S)$  have been estimated by using the intrinsic colour relation of early type stars, given by S13 (see their ta-

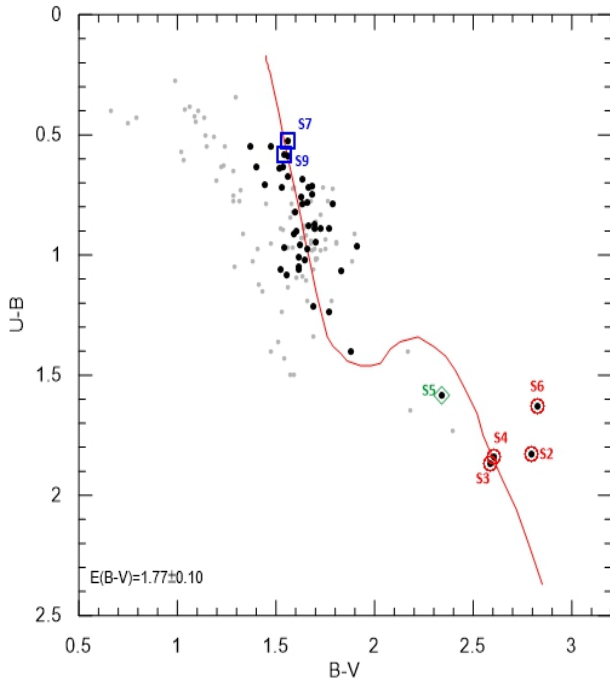


**Figure 7.**  $(U - B), (B - V)$  (CC) diagram for 38 members (filled dots) of Be 55. Grey symbols denote the 97 stars from Maidanak  $UBV$  CCD observations. Red curve shows the reddened SK82 main sequence. The symbols of bright evolved stars are the same as Fig. 6.

bles 2–3). Here the colour excess ratio  $E(U - B) = 0.72E(B - V) + 0.025E(B - V)^2$  of S13 is adopted. The reddening law of Be 55 using colour excess ratios  $E(V - \lambda)$  for IJHK<sub>S</sub> photometry has been tested in Fig. 8. 38 members (filled blue dots) lie on the solid line. The total-to-selective extinction ratio is obtained as  $R_V = 3.13 \pm 0.04$  (Table 4), which implies that the reddening law toward Be 55 is quite normal. According to Guetter & Vrba (1989), colour excess ratio of optical-near infrared colours is related to the total-to-selective extinction ratio.

Its highly reddened value,  $E(B - V) = 1.77 \pm 0.10$  mag is in agreement with  $E(B - V) = 1.85$  mag of N12,  $E(B - V) = 1.81 \pm 0.15$  mag of A20,  $E(B - V) = 1.75$  mag of Molina Lera et al. (2018),  $E(B - V) = 1.74$  mag of L18, and  $E(B - V) = 1.74 \pm 0.10$  mag of Maciejewski & Niedzielski (2007) within the uncertainties (Table 7), respectively. This reddening is larger than the ones of Tadross (2008) and Bukowiecki et al. (2011). Note that N12 also give  $E(J - K_S) = 0.85$  mag, which converts to  $E(B - V) = 1.73$  mag via a relation  $E(J - K_S) = 0.49E(B - V)$  of Dutra et al. (2002).

The reddening value derived from the early type stars cannot be used to deredden late-type supergiants. Therefore, the mean reddening value from their  $(J - K_S)$

**Table 4.**  $E(V - \lambda)/E(B - V)$  ratios (Col. 2) in terms of four colour indices (Col. 1).  $R_V$  is the weighted average of four colours. Here  $\lambda$  is I, J, H and  $K_S$ . N (last column): cluster star numbers.

Colour	$E(V - \lambda)/E(B - V)$	N
V-I	$1.300 \pm 0.050$	38
V-J	$2.341 \pm 0.131$	38
V-H	$2.659 \pm 0.172$	38
V- $K_S$	$2.841 \pm 0.177$	38
$R_V = 3.13 \pm 0.04$		

colours of the five evolved stars (Table 5) is estimated as  $E(J - K_S) = 0.92 \pm 0.06$  mag, by utilising the intrinsic colour,  $(J - K_S)_0$  of Koornneef (1983). This converts to  $E(B - V) = 1.84 \pm 0.11$  mag from the relation  $E(J - K_S) = 0.49E(B - V)$  (Dutra et al., 2002). Their reddenings are listed in Col. 5 of Table 5. For Be 55, A20 mention a non-negligible differential reddening. The reddened values  $E(B - V) = 1.77 \pm 0.10$  mag (early type stars) and  $E(B - V) = 1.84 \pm 0.11$  mag (five evolved stars) imply a differential reddening in Be 55. The members selected in Fig. 7 are scattered over more than 0.3 mag in  $(B - V)$  for a given  $(U - B)$ . Likewise, the members are scattered over more than 0.5 mag in  $(G, G_{BP} - G_{RP})$  (Fig. 4).

The spatial variation of reddening of Be 55 as the reddening map, is derived from its member stars (red dots) and field stars (black dots), and is presented in Fig. 9. The size of the dots is scaled to the magnitude of the star. The coloured line types as iso-reddening contours represent different amounts of reddening  $E(B - V)$ . From Fig. 9, there seems to be a differential reddening across the cluster due to a slight variation of  $E(B - V)$ . Most young OCs with ages younger than 10 Myr show a differential reddening across the field of view. But for slightly old OCs, it is not well known whether there is a differential reddening across the cluster or not. That's the reason to check the differential reddening across the cluster.

### 3.4 Distance

Instead of the reddening-corrected CMDs, distance modulus/distance of Be 55 is obtained by using the ZAMS fitting method with the reddening-independent indices (S13). For this,  $UBVRIJHK_S$  photometry of 38 early type stars is used. The reddening-independent quantities,  $Q', Q_{VI}, Q_{VJ}, Q_{VH}$  and  $Q_{VK_S}$  are utilised. The  $Q_{V\lambda} - Q'$  plots for 38 early type members have been displayed in Fig. 10. Solid lines denote the fitted ZAMS relation of Sung et al. (2013) to the members. As sug-

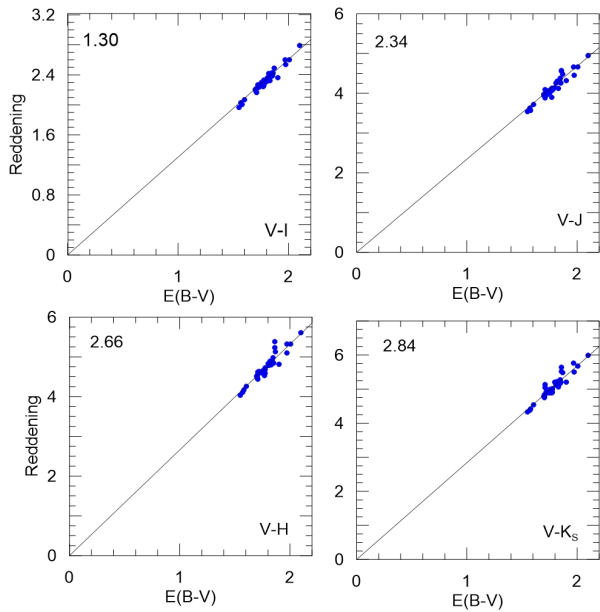


**Figure 8.**  $E(V - \lambda)$  versus  $E(B-V)$  relations.  $\lambda$  denotes IJHK<sub>S</sub> photometry. The solid line means  $R_V = 3.1$ . The colour excess ratios from the IJHK<sub>S</sub> data consistently show that the reddening law toward Be 55 is normal.

gested by Lim et al. (2014), ZAMS should be fitted to the lower ridge of the MS band to avoid the effects of multiplicity and evolution. The ZAMS line is shifted up and down in Fig. 10 by 0.1 mag. The error of this method is about 0.20 mag. Once the ZAMS has been adjusted above and below the distribution of the members (Fig. 10), the distance modulus from four colour indices is obtained as  $(V_0 - M_V) = 12.40 \pm 0.20$  mag, equivalent to  $3.02 \pm 0.28$  kpc, which are adopted for this paper. The median Gaia EDR3 parallax is  $\varpi = 0.317 \pm 0.059$  mas, which corresponds to  $(V_0 - M_V) = 12.49 \pm 0.41$  mag ( $d = 3.15 \pm 0.59$  kpc). The two distances

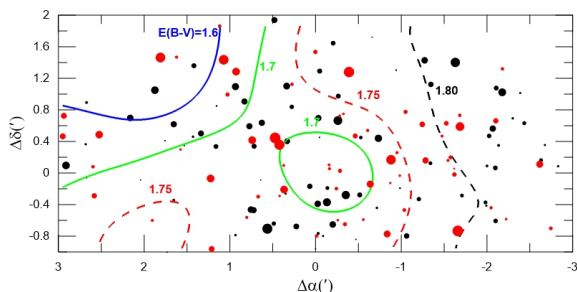


**Figure 9.** Reddening map of Be 55. Red and black dots shows the member and the field stars, respectively. The size of the dots is scaled to the magnitude of the star. The coloured line types as iso-reddening contours represent different amounts of reddening  $E(B - V)$ .

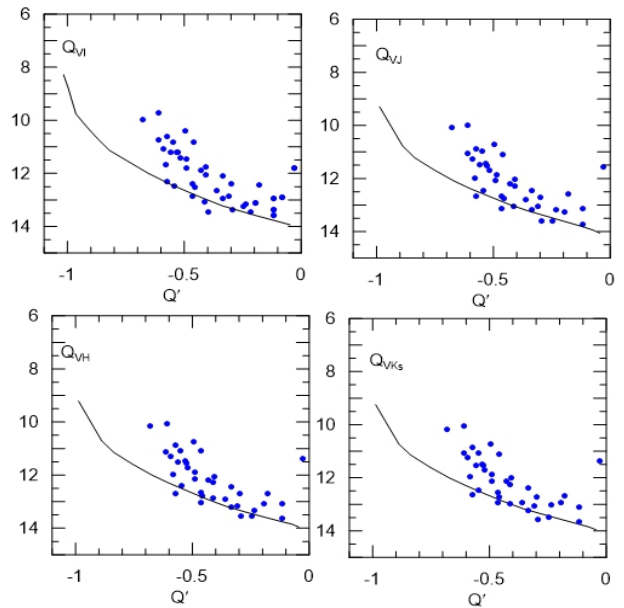


**Figure 10.**  $Q_{V,\lambda}$  versus  $Q'$  diagrams (38 early type members, filled blue dots) for determination of distance modulus of Be 55.  $\lambda$  denotes IJHK<sub>S</sub> filters. A careful ZAMS fitting to the lower boundary of the MS band was carried out in the reddening-independent  $Q_{V,\lambda}$ - $Q'$  planes. The ZAMS relation of S13 is used to determine the distance to the cluster after adjusting by  $12.4 \pm 0.2$ , respectively.

are compatible within the uncertainties.

#### 4. Age of Be 55

$M_{bol} - \log T_{eff}$  diagram (HRD) for 46 members (41 early type and five RSGs/RBGs) is presented in Fig. 11. Their effective temperature and  $BC$  values have been determined from their  $(U - B)_0$  and  $(B - V)_0$  by utilising table 5 of S13. Their  $M_{bol}$  values are obtained from the relation  $M_{bol} = BC + V - R_V E(B - V) - (V_0 - M_V)$ . For this, the UB<sub>V</sub> photometry of 41 early type and five RSGs/RBGs is de-reddened by  $E(B - V) = 1.77$  mag and  $E(B - V) = 1.84$  mag, respectively.

The metal abundance,  $[M/H] = 0.07 \pm 0.12$  ( $Z = 0.014$ ) of Be 55, given by L18 is considered for selecting the isochrone. Note that Be 55 has a extended main sequence. Due to the diversity of the rotational velocity even in a cluster (Lim et al. , 2019), MS turn-off broadens. Broadening in the main sequence of the CMD could be also due to binarity, peculiarity, rotation in the stars. Therefore, the solar abundance Geneva models of Ekström et al. (2012) (hereafter E12) ( $V/V_{crit} = 0.4$ ) and Georgy et al. (2013) (hereafter G13) (for B-type stars and  $V/V_{crit} = 0.3$ ) have been fitted to the members in the  $M_{bol} - \log T_{eff}$  (Fig. 11) and de-reddened  $(V_0, B -$

**Table 5.** Properties of seven bright stars in Be 55.

Star no (N12/L18)	V mag	(B-V)	(U-B)	E(J-K <sub>s</sub> )/E(B-V)	<i>m</i> (M <sub>⊙</sub> )	M <sub>V</sub> mag	$\varpi$ mas	<i>d</i> <sub>Gaia</sub> kpc	<i>d</i> <sub>ph.</sub> kpc	SpT (A20)
S5/L107	14.106	2.340	1.582	0.863/1.726	5.9	-3.99	0.324±0.017	3.09±0.16	3.47±0.45	F8Ib
S3/L163	14.754	2.588	1.866	0.933/1.866	5.8	-3.35	0.360±0.015	2.78±0.12	2.84±0.37	G8II
S4/L110	14.437	2.604	1.840	0.885/1.770	5.9	-3.67	0.305±0.022	3.28±0.24	3.26±0.42	K0Ib-II
S2/L196	14.094	2.796	1.826	1.006/2.012	6.0	-4.01	0.294±0.024	3.40±0.28	2.30±0.30	K0Ib
S6/L145	14.266	2.825	1.628	0.906/1.812	6.0	-3.84	0.402±0.029	2.49±0.18	3.07±0.40	K4II
S9/L198	15.186	1.562	0.524	-/1.770	7.5	-2.70	0.297±0.016	3.37±0.18	2.95±0.38	B3-4IIIShell
S7/L94	14.666	1.543	0.581	-/1.770	7.5	-3.22	0.334±0.014	2.99±0.13	2.95±0.38	B4IV

$V_0$ ) (Fig. 12).  $(V_0 - M_V) = 12.40 \pm 0.20$  mag (Q technique) and the reddenings  $E(B - V) = 1.77 \pm 0.10$  mag (for early type stars) and  $E(B - V) = 1.84 \pm 0.11$  mag (for evolved stars) have been applied to the E12 and G13 isochrones while fitting.

As is seen in Fig. 11, the  $85 \pm 13$  Myr E12 isochrone with high rotation (blue curve) describes general morphology of HRD without accurate locations. The 85 Myr E12 isochrone (blue curve) is almost consistent with the RSGs/RBGs, S4/L110, S5/L107 (Cepheid), and S6/L145, except for S3/L163. Also, the  $70 \pm 10$  Myr G13 isochrone (red curve) with moderate rotation for B-type stars provides good fit with the RSGs/RBGs, S2/L196, S4/L110 and S5/L107 (Cepheid), except for S3/L163 and S6/L145. Note that S5/L107 appears to be on the core-He burning blue loop. Note that non-rotating E12 isochrone (blue dashed line) gives a faint turn-off, and going below the RSGs/RBGs.

On the  $V_0 - (B - V)_0$  (Fig. 12), S2/L196 and three RSGs/RBGs occupy positions which are consistent with the 85 Myr E12 isochrone. However, the 70 Myr G13 isochrone is not compatible with the positions of the RSGs/RBGs.

The two BSs, S9/L198 and S7/L94 locate between ZAMS and the 45 Myr isochrone (Figs. 11-12). The age of BSs seems to be definitely younger than the cluster. From Figs. 11-12, there appears an extended main-sequence turn-off (eMSTO), since the main sequence band is expected to broaden in CMDs due to their different main sequence lifetimes. Also, the broadening in the MS band may also be due to differential reddening across the cluster because the scatter in  $E(B - V)$  is about 0.1 mag (section 3.3). One can expect about 0.3 mag scatter ( $3\sigma$ ), since the width of MS band is about 0.3 mag.

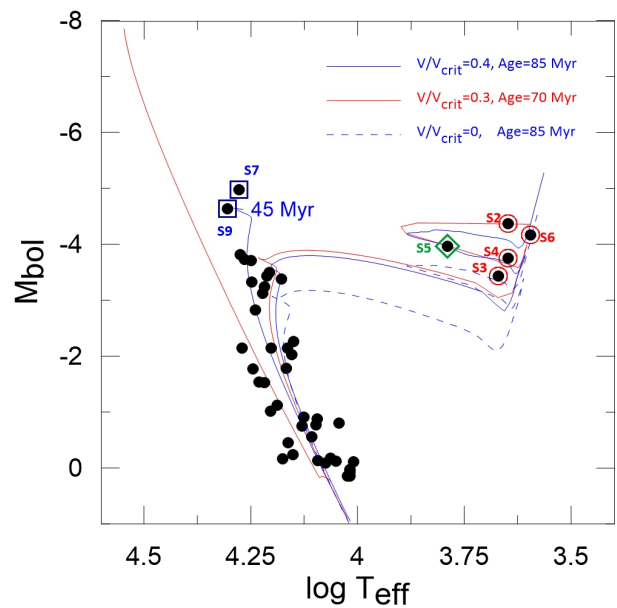


**Figure 11.**  $M_{bol}$  versus  $\log T_{eff}$  of 46 probable members. Solid and dashed blue curves represent rotating/non-rotating E12 isochrones. Red curve shows G13 isochrone for B type stars with  $V/V_{crit} = 0.3$ . The solid red line represents the ZAMS of E12. The symbols are the same as Fig. 6.

## 5. Kinematics and orbital parameters

From the radial velocities of A20 and the Gaia EDR3 proper motions for five RSGs/RBGs, their heliocentric velocities ( $U, V, W$ ) in the right-hand system have been calculated from the algorithm of Johnson and Soderblom (1987). The photometric distance of Be 55 ( $3.02 \pm 0.28$  kpc) is adopted, instead of their individual parallaxes. These space velocities are transformed to the components  $U', V', W'$  by correcting for the Solar motion  $(U, V, W)_\odot = (+11.10, +12.24, +7.25)$  km s<sup>-1</sup> with respect to the local standard of rest (LSR) Schönrich and Binney (2010). Here,  $R_\odot = 8.2 \pm 0.1$  kpc



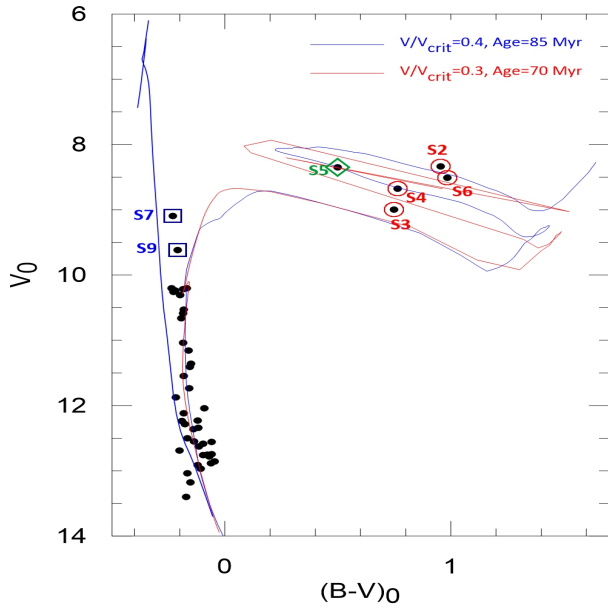


**Figure 12.**  $V_0$ - $(B - V)_0$  of 46 probable members. The symbols are the same as Fig. 11.

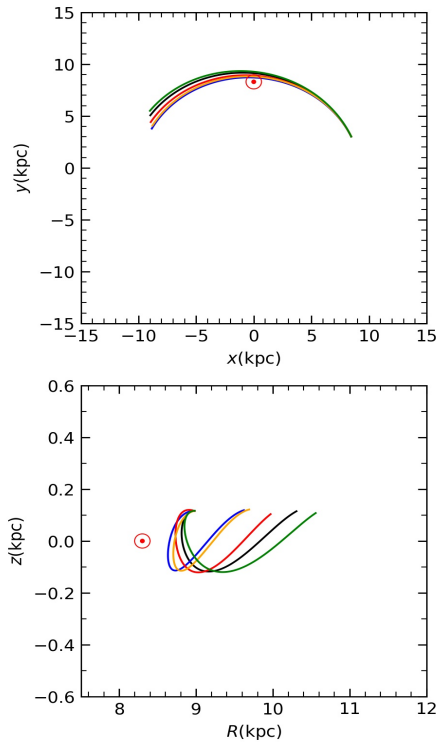


**Figure 13.** The orbits of five RSGs/RBGs on  $x$ - $y$  (kpc) (top panel) and  $z$ - $R$  (kpc) (bottom panel). Large circle shows the position of the Sun,  $(z_\odot, R_\odot) = (0, 8.2 \text{ kpc})$ .

(Brunthaler et al. , 2011) are adopted. The heliocentric cartesian distances  $(x', y', z')$  (kpc) and LRS-velocity components  $(U', V', W')$  have been transformed to Galactic Rest of Frame (GSR) i.e.,  $(x, y, z)$  (kpc) and  $(V_x, V_y, V_z)$  from the equations of Kepley et al. (2007). The Galactocentric velocity component  $(V_\Phi)$  ( $\text{km s}^{-1}$ ) (or azimuthal velocity) in a cylindrical frame is estimated via  $V_\Phi = \frac{xV_y - yV_x}{R}$ . Here,  $V_\Phi < 0$  means prograde. By utilising the "MWPotential2014" code in the galpy-code library<sup>1</sup> written by Bovy (2015), peri- and apo-galactic distances  $(R_{min}, R_{max})$  (kpc) and the maximum height distance  $(z_{max})$  (kpc) have been obtained. The orbital eccentricity (ecc) is estimated via the relation  $e = (R_{max} - R_{min}) / (R_{max} + R_{min})$ . Five evolved member's orbits have been integrated for 85 Myr within the Galactic potential. The galactic potential as sum of the Galactic components is explained by Bovy (2015). Their orbital angular momentum components  $J_x, J_y, J_z$  and  $J_\perp$  ( $\text{kpc km s}^{-1}$ ) are calculated from the equations of Kepley et al. (2007). The total angular momentum  $J_\perp$  is defined as  $J_\perp = (J_x^2 + J_y^2)^{1/2}$ . The relations of  $x$ - $y$  (kpc) and  $z$  -  $R$  (kpc) of the five RSGs/RBGs are shown in Fig. 13.

**Table 6.** For the available Gaia EDR3 proper motion components ( $\text{mas yr}^{-1}$ ) and spectroscopic radial velocity data ( $\text{km s}^{-1}$ ) of five RSGs/RBGs, kinematics  $(U, V, W, V_\Phi)$   $\text{km s}^{-1}$ , orbital parameters  $(R_{max}, R_{min}, z_{max})$  (kpc), eccentricity (ecc), and angular momentums  $(J_z$  and  $J_\perp)$  ( $\text{kpc km s}^{-1}$ ), respectively.

Star	$\mu_\alpha$	$\mu_\delta$	$V_{rad}$
S2	$-4.020 \pm 0.029$	$-4.816 \pm 0.027$	$-24.55 \pm 0.39$
S3	$-4.043 \pm 0.017$	$-4.743 \pm 0.016$	$-33.33 \pm 0.47$
S4	$-4.176 \pm 0.025$	$-4.687 \pm 0.024$	$-28.97 \pm 0.47$
S5	$-3.907 \pm 0.020$	$-4.716 \pm 0.018$	$-31.63 \pm 0.86$
S6	$-4.043 \pm 0.033$	$-4.813 \pm 0.031$	$-21.61 \pm 0.60$

	U	V	W	$V_\Phi$
S2	90.71	-19.59	-7.55	-252.38
S3	90.66	-28.39	-6.88	-244.08
S4	91.18	-24.04	-4.84	-248.35
S5	88.94	-26.72	-7.97	-245.07
S6	90.76	-16.60	-7.23	-255.22

	$R_{min}$	$R_{max}$	ecc
S2	8.81	10.31	0.08
S3	8.63	9.62	0.05
S4	8.73	9.97	0.07
S5	8.70	9.69	0.05
S6	8.85	10.56	0.09

	$z_{max}$	$J_z$	$J_\perp$
S2	0.12	-2266	24
S3	0.12	-2192	24
S4	0.12	-2230	33
S5	0.12	-2200	24
S6	0.13	-2292	24

<sup>1</sup><http://github.com/jobovy/galpy>

(Bland-Hawthorn et al. , 2016) and  $V_{LSR} = 239 \text{ km s}^{-1}$

**Table 7.** Comparison with the literature for Be 55.

E(B-V) mag	$(V_0 - M_V)$ mag	$d$ (kpc) kpc	$Z$	$\log \text{Age}$	Age Myr	Isochrone	Photometry	Ref.
1.77±0.10	12.40±0.20	3.02±0.28	0.014	7.93±0.06	85±13	Ekström et al. (2012)	CCD <i>UBVI</i>	This paper
1.74±0.07	11.71±0.30	2.20±0.30		7.80	63±12	PLR of S5 Cepheid	CCD <i>VR</i>	Lohr et al. (2018)
1.85±0.16	13.0±0.30	3.98±0.55	solar	7.70	50±10	Marigo et al. (2008)	CCD <i>UBV</i>	Negueruela & Marco (2012)
1.81±0.15	12.55±0.15	3.24±0.22	solar	7.80±0.10	63±15	Ekström et al. (2012)	CCD <i>UBV</i>	Alonso-Santiago et al. (2020)
1.75	12.40	3.02	solar	7.50-8.50	30-100	Bressan et al. (2012)	<i>ugr</i>	Molina Lera et al. (2018)
1.74±0.10	10.42	1.21±0.31	solar	8.50	315	Bertelli (1994)	CCD <i>BV</i>	Maciejewski & Niedzielski (2007)
1.50		1.44±0.07	solar	8.48	300	Bonatto et al. (2004)	2 <i>MAS</i> – <i>JHK<sub>s</sub></i>	Tadross (2008)
1.15	12.23	1.70±0.13	0.019	8.95	891	Girardi et al. (2002)	2 <i>MAS</i> – <i>JK<sub>s</sub></i>	Bukowiecki et al. (2011)
1.55( $A_V = 4.8$ )	12.20	2.75	0.015	8.30	200	Bressan et al. (2012)	<i>Gaia DR2</i>	Cantat-Gaudin et al. (2018, 2020)

**Table 8.** Distances for the values of  $V$ ,  $M_V$ ,  $P = 5.85$  day, and  $E(B - V)$  of Cepheid S5. The methods and their references for  $M_V$  are listed in Cols.5–6.

$d$ kpc	$V$ mag	$M_V$ mag	$E(B - V)$ mag	Methods for $M_V$	Ref.	Remarks
3.47±0.45	14.106	-3.99	1.73	E12 isochrone	1	This paper
2.78±0.32	14.106	-3.52	1.73	$-(2.67±0.16)(\log P - 1) - (4.14±0.05)$	2	This paper
3.09±0.16						Gaia EDR3
2.20±0.30	13.834	-3.23	1.74	$-(2.88±0.18)\log P - (1.02±0.16)$	3	L18
2.40±0.30	13.834	-3.93	1.74	$-(2.43±0.12)(\log P - 1) - (4.5±0.02)$	4	L18
3.03±0.37	13.834		1.81	$a(\log P - 1) + b$ , for JHK	5	A20

Table Notes. [1]:Ekström et al. (2012), [2]: Lazovik and Rastorguev (2020), [3]: Anderson et al. (2013), [4]:Benedict et al. (2007), [5]:Chen et al. (2017).

## 6. Discussion and Conclusion

The photometric distance modulus/distance of Be 55 as  $(V_0 - M_V) = 12.40 \pm 0.20$  mag ( $3.02 \pm 0.28$  kpc) is better and well consistent with the median Gaia EDR3 distance ( $3.15 \pm 0.59$  kpc). These distances locate Be 55 near the Perseus Spiral arm. The photometric distance of this paper is in concordance with  $3.24 \pm 0.22$  kpc of A20 and 3.02 kpc of Molina Lera et al. (2018) (Table 7). It is rather smaller than N12 but is farther than L18. L18's distance is from period-luminosity relation (PLR) of Cepheid S5 (Table 8). N12 obtain its distance modulus from the dereddened ZAMS of Mermilliod (1981) and SK82 as  $13.0 \pm 0.30$  mag on  $M_V - (B - V)$ . This corresponds to a distance,  $3.98 \pm 0.55$  kpc. L18's distance locates Be 55 on the outer edge of Local arm rather than in the Perseus arm as N12 suggest. A mismatch between the distances of L18 and N12 is explained by the underestimated uncertainties in N12's distance modulus. The other literature give close distances.

The distance 2.78 kpc of Cepheid S5/L107, from the PLR of Lazovik and Rastorguev (2020) is consistent with the ones of Gaia EDR3 and A20 within the errors (Table 8). Note that L18 give close distances.  $M_V = -3.99$  from E12 isochrone estimates a large distance, 3.47 kpc.

The E12 isochrone (high rotation) fittings to

HRD/CMD derive turn-off age,  $85 \pm 13$  Myr of Be 55, by taking care five RSGs/RBGs. For this age, the masses of five RSGs/RBGs from the E12 isochrone are about  $6 M_\odot$  (Col. 6 of Table 5). The 70 Myr G13 isochrone with moderate rotation does not provide a good fit to the RSGs/RBGs on the  $V_0 - (B - V)_0$  (Fig.12). The age 85 Myr is somewhat older than N12, L18, and A20 (Table 7) but falls in the range of 30–100 Myr of Molina Lera et al. (2018). From the non-rotating PARSEC isochrones, A20 give its age as  $63 \pm 15$  Myr (see their fig. 6 and table 1), by considering evolved members. The age 85 Myr also falls in the range of 63–105 Myr, which is found from the period-age relations in table 14 of A20 for Cepheid S5/#107. Note that N12 apply two isochrones of Marigo et al. (2008);  $\log t = 7.6$  (40 Myr) and  $\log t = 7.7$  (50 Myr) on  $(V, U - B)$ . By taking  $E(J - K_S) = 0.85$  mag, N12 also apply the same isochrones to  $(K_S, J - K_S)$ , and give an age 50 Myr. The other literature values find more old ages (Table 7), than this paper.

From Table 7, Note that Cantat-Gaudin et al. (2018, 2020) from Gaia DR2 photometry give a less reddening, a close distance and an old age, 200 Myr, as compared to the values of this paper.

The spread of the brightness of the RSGs/RBGs in the HRD/CMDs indicates a much large spread in age. This feature may be the result of the diversity of stellar rotation among evolved cluster members (Lim et al. , 2019; Lim et al., 2016; Sung et al., 1997), which indicate the necessity of cluster isochrone with non-single rotational velocity distribution. The stars in OCs do not have the same rotational velocity (Lim et al. , 2019). Some stars have very low rotational velocities, and some may be fast rotators. For that case, even the same mass stars are not the same position in the HRD because fast rotators have longer MS lifetime. This feature also indicates the necessity of cluster isochrones with non-single rotational velocity distribution. As a result, the possible inconsistencies on the locations of the RSGs/RBGs to the rotating/non-rotating isochrones may be resulting from the age spread of stars in young

OCs. According to A20, the possible inconsistency of the locations of the RSGs/RBGs on HRD/CMD is due to the strong reddening, rather than metal abundance.

Two BS candidates in  $V_0-(B-V)_0$  (Fig. 12) lie on ( $V_0 < 10.01 \text{ mag}$ ) ( $V < 15.50 \text{ mag}$ ) and ( $(B-V)_0 < 0.03$ ) ( $(B-V) < 1.80$ ). These limits for  $V_0$  and  $(B-V)_0$  which BSs occupy in CMDs are similar to those given by Carney (2001, fig. 19) and Carraro et al. (2010, fig. 10). The positions of two BSs locate between ZAMS and the 85 Myr isochrone. The age of BSs is definitely younger than the cluster. Therefore the 45 Myr isochrone is drawn up to MS turn-off. As discussed by Ferraro (2016), BSs are commonly defined as stars brighter and bluer than the main-sequence (MS) turnoff in open/globular clusters. Therefore, their origin cannot be explained with normal single star evolution. Two main formation mechanisms are proposed: (1) mass transfer in binary systems (McCrea, 1964) possibly up to the complete coalescence of the two stars, and (2) stellar collisions (Hills and Day, 1976). Both these processes can potentially bring new hydrogen into the core and therefore 'rejuvenate' a star to its MS stage (Lombardi et al., 2002; Chen and Han, 2009). According to Sandage (1953) and Tout et al. (1997), the increase in mass of a star makes it look younger than it is.

The kinematics, orbital and angular momentum values of the five evolved members (Table 6) indicate that Be 55 is a member of Galactic thin disk population, which is also consistent with its metallicity,  $[M/H] = 0.07 \pm 0.12$ . With the circular orbits,  $\text{ecc} = [0.05, 0.09]$ , Be 55 does not seem to be completed a tour around the center of the Galaxy (top panel of Fig. 13). They reach to  $z \sim 0.13 \text{ kpc}$ , and their birth places are at  $\sim 9 \text{ kpc}$  (bottom panel of Fig. 13). However, their orbits show that the cluster passed a part of its time at  $R_{\text{min}} = 8.63 - 8.85 \text{ kpc}$ .

The total mass for 64 early type members is obtained as  $M_{\text{tot}} = 224 M_{\odot}$  from 85 Myr E12 isochrone. From the photometric distance ( $3.02 \pm 0.28 \text{ kpc}$ ) and angular size  $\theta \sim 0.073 \text{ deg}$  ( $0.0013 \text{ rad}$ ), the diameter of Be 55 is determined as  $3.85 \text{ pc}$ . In order to check its stability, the maximum tangential velocity of the members within the radius of  $\mu = 0.5 \text{ mas yr}^{-1}$  is estimated as  $7.2 \text{ km s}^{-1}$ , via the relation,  $V_{\text{tan}} = 4.74\mu \times d(\text{kpc})$ . These values indicate that its virial mass is about  $M_{\text{vir}} = 25100 M_{\odot}$ , which is far larger than the cluster mass,  $224 M_{\odot}$ . Be 55 with its total mass,  $224 M_{\odot}$ , depending on its location of  $R_{\text{GC}} = 9.04 \text{ kpc}$  and  $\ell = 93^{\circ}.03$  is a survivor against internal and external perturbations related to, e.g. stellar evolution, mass segregation, spiral arms, and encounters with the disk and giant molecular clouds.

## Acknowledgements

I thank H. Sung for providing his private photometric data, and the interpretations on the analysis. Y. Karatas and H. Cakmak are also thanked for the kinematics and dynamics. The referee is thanked for the useful suggestions. This paper has made use of results from the European Space Agency (ESA) space mission Gaia, the data from which were processed by the Gaia Data Processing and Analysis Consortium (DPAC). Funding for the DPAC has been provided by national institutions, in particular the institutions participating in the Gaia Multilateral Agreement. The Gaia mission website is <http://www.cosmos.esa.int/gaia>.

## References

- Akkaya Oralhan, Í., Michel, R., Schuster, W.J., Karataş, Y., Karşlı, Y., Chavarría-K, C., 2019, Journal of Astrophysics and Astronomy, 40,33
- Akkaya Oralhan, Í., Michel, R., Karşlı, Y., Cakmak, H., Sung, H., Karataş, Y, 2020, Astronomische Nachrichten, 341, 44
- Alonso-Santiago, J., Negueruela, I., Marco, A., Tabernero, H.M., Gonzalez-Fernandez,C., Castro, N., 2017, MNRAS, 469, 1330
- Alonso-Santiago, J., Negueruela, I., Marco, A., Tabernero, H.M., and Castro, N., 2020, arXiv:2009.124118v, Astronomy and Astrophysics, ?? (A20)
- Anderson, R.I., Eyer, L., Mowlavi, N., 2013, MNRAS, 434, 2238
- Arellano Ferro, A., Giridhar, S., Rojo, Arellano, E., 2003, RevMexAA, 39, 3
- Bastian N., de Mink S. E., 2009, MNRAS, 398, L11
- Benedict, G.F. et al., 2007, Astronomical Journal, 133, 1810
- Bertelli, G., Bressan, A., Chiosi, C., Fagotto, F., & Nasi, E., 1994, A&AS, 106, 275
- Bland-Hawthorn, J. and Ortwin Gerhard, O. 2016, Annual Review of Astron and Astrophys, 54, 529
- Bonatto Ch., Bica E., Girardi L., 2004, Astronomy and Astrophysics, 415, 571
- Bonatto, Ch., Bica, E., 2007, Astronomy and Astrophysics, 473, 445
- Bovy, J., 2015, ApJS, 216, 29
- Bressan A., Marigo, P., Girardi L., Salasnich, B., Dal Cero, C., Rubele, S., Nanni, A., 2012, MNRAS, 427, 127
- Brown, A. G. A., Vallenari, A., Prusti, T. et al., 2018, Astronomy and Astrophysics, 616, 1G
- Brown, A. G. A., Vallenari, A., Prusti, T. et al., 2020, arXiv:201201533G

- Brunthaler, A., Reid, M.J., Menten, K.M., et al. 2011, *AN*, 332, No.5, 461
- Bukowiecki, L., Maciejewski, G., Konorski, P., Strobel, A., 2011, *AcA* 61, 231
- Cantat-Gaudin, T., Jordi, C., Vallenari, A., Bragaglia, A., Balaguer-Nunez, L., Soubiran, C., Bossini, D., Moitinho, A., Castro-Ginard, A., Krone-Martins, A., and 3 coauthors., 2018, *Astronomy and Astrophysics*, 618, 93
- Cantat-Gaudin, T., Anders, F., Castro-Ginard, A., Jordi, C., Romero-Gómez, M., Soubiran, C., Casamiquela, L., Tarricq, Y., Moitinho, A., Vallenari, A., Bragaglia, A., Krone-Martins, A., Kounkel, M., 2020, *Astronomy and Astrophysics*, 640, 1
- Carney, B. 2001, *Star Clusters*, Saas-Fee Advanced Course 28, Lecture Notes 1998, Swiss Society for Astrophysics and Astronomy, eds. L. Labhardt and B. Binggeli (Berlin: Springer-Verlag) pp. 1-222
- Carraro, G., Costa, E., Ahumada, J.A., 2010, *Astronomical Journal*, 140, 954
- Chen, X. F. and Han, Z. W., 2009, *MNRAS*, 395, 1822
- Chen, X., de Grijs, R., Deng, L., 2010, *MNRAS*, 404, 119
- Chiosi, C., Bertelli, G., Bressan, A., 1992, *Annual Review of Astron and Astrophys*, 30, 235
- Dutra, C.M., Santiago, B.X., Bica, E., 2002, *Astronomy and Astrophysics*, 383, 219
- Ekström, S., Georgy, C., Eggenberger, P., Meynet, G., Mowlavi, N., Wyttenbach, A., Granada, A., Decressin, T., Hirschi, R., Frischknecht, U., Charbonnel, C., Maeder, A., *Astronomy and Astrophysics*, 2012, 537,146 (E12)
- Fernie, J.D., 1963, *Astronomical Journal*, 68, 780
- Ferraro, F.R., 2016, *Star Clusters and Black Holes in Galaxies across Cosmic Time*, Proceedings of the International Astronomical Union, IAU Symposium, Volume 312, pp. 171-180.
- Florentino, G., Lanzoni, B., Dalessandro, E., et al., 2014, *Astrophysical Journal*, 783, 34
- Fitzgerald, M.P., 1970, *Astronomy and Astrophysics*, 4, 234
- Gilliland, R. L., Bono, G., Edmonds, P. D., et al., 1998, *Astrophysical Journal*, 507, 818
- Girardi, L., Bertelli, G., Bressan, A., Chiosi, C., Groenewegen, M.A.T., Marigo, P., Salasnich, B., Weiss, A., 2002, *Astronomy and Astrophysics*, 391, 195
- Georgy, C., Ekström, S., Granada, A., Meynet, G., Mowlavi, N., Eggenberger, P., Maeder, 2013, *Astronomy and Astrophysics*, 553, 24 (G13)
- Guetter, H. H., & Vrba, F. J. 1989, *Astronomical Journal*, 98, 611
- Hills, J. and Day, C., 1976, *Astron. Lett.*, 17, 87
- Johnson, D. R. H., & Soderblom, D. R., 1987, *Astronomical Journal*, 93, 864
- Kepley, A., Morrison, H.L., Helmi, A., Kinman, T.D., et al., 2007, *Astronomical Journal*, 134, 1579
- Kharchenko, N.V., Piskunov, A.E., Schilbach, E., Röser, S., Scholz, R.D., 2013, *Astronomy and Astrophysics*, 558, 53
- Kilkenny, D., Van Wyk, F., Roberts, G., Marang, F., Cooper, D., 1998, *MNRAS*, 294, 93
- King, I., 1966, *Astronomical Journal*, 71, 64
- Koornneef, J., 1983, *Astronomy and Astrophysics*, 128, 84
- Lazovik, Y.A., Rastorguev, A.S., 2020, *Astronomical Journal*, 160, 2020
- Li, C., de Grijs R., Deng L., Milone A. P., 2017, *Astrophysical Journal*, 844, 119
- Lim, B., Sung, H., Bessell, M. S., Karimov, R., Ibrahimov, M. 2009, *JKAS*, 41, 161
- Lim, B., Sung, H., Kim, J.S., Bessell, M., Park, B-G., 2014, *MNRAS*, 443, 454
- Lim, B., Sung, H., Kim, J.S., Bessell, M.S., Hwang, N., Park, B-G. 2016, *Astrophysical Journal*, 831, 116
- Lim, B., Rauw, G., Nazé, Y., Sung, H., Hwang, N., Park, B-G., 2019, *NatAs*, 3, 76
- Lindgren, L., Hernandez, J., Bombrun, A., Klioner, S. et al., 2018, *Astronomy and Astrophysics*, 616, A2
- Lindgren, L., Hernandez, J., Bombrun, A., Klioner, S. et al., 2020, 2020arXiv201201533G
- Lohr, M. E., Negueruela, I., Tabernero, H. M., Clark, J. S., Lewis, F. and Roche, P. 2018, *MNRAS*, 478, 3825 (L18)
- Lombardi, Jr., J. C., Warren, J. S., Rasio, F. A., Sills, A., and Warren, A. R., 2002, *Astrophysical Journal*, 568, 939
- Maciejewski, G., & Niedzielski, A. 2007, *Astronomy and Astrophysics*, 467, 1065
- McCrea, W. H., 1964, *MNRAS*, 128, 147
- Marco, A., Negueruela, I., Gonzalez-Fernandez, C., Maiz Apellaniz, J., Dorda, R., Clark, J.S., 2014, *Astronomy and Astrophysics*, 567, 73
- Marigo, P., Girardi, L., Bressan, A., et al., 2008, *Astronomy and Astrophysics*, 482, 883
- Mermilliod, J.-C., 1981, *Astronomy and Astrophysics*, 97, 235
- Menzies, J. W., Marang, F., Laing, J. D., Coulson, I. M., Engelbrecht, C. A., 1991, *MNRAS*, 248, 642
- Molina Lera, J.A, Baume, G., Gamen, R., 2018, *MNRAS*, 480, 2386
- Negueruela, I., & Marco, A. 2012, *Astronomical Journal*, 143, 46 (N12)
- Negueruela, I., Clark, J. S., Dorda, R., González-Fernández, C., Marco, A., Monguio, M., 2016, Vol.507, page 75 , Edited by Ian Skillen, Marc Balcells, and Scott Trager. ASP Conference Series, San Francisco: Astronomical Society of the Pacific (ASPC).

- Negueruela, I., Monguio, M., Marco, A., Tabernero, H.M., Gonzalez-Fernandez, C., Dorda, R., 2018, *MNRAS*, 477,2976
- Sampedro, L., Dias, W.S., Alfaro, E.J., Monteiro, H., Molina, A., 2017, *MNRAS*, 470, 3937
- Sandage, A.R., 1953, *Astronomical Journal*, 58, 61
- Schmidt-Kaler, Th. 1982, in Landolt-Bornstein, Numerical Data and Functional Relationships in Science and Technology, New Series, Group VI, Vol.2b, eds. K. Schaifers & H. H. Voigt (Berlin: Springer), p. 14 (SK82)
- Schönrich R., Binney J., Dehnen, W., 2010, *MNRAS*, 403, 1829
- Sung, H., Bessell, M.S., See-Woo, L., 1997, *Astronomical Journal*, 114, 2644
- Sung, H., & Bessell, M. S. 1999, *MNRAS*, 306, 361
- Sung, H., Lim, B., Bessell, M.S. Kim, J.S., Hur, H., Chun, M-Y., Park, B-G., 2013, *JKAS*, 46, 97 (S13)
- Tadross, A. L. 2008, *MNRAS*, 389, 285
- Tout, C. A., Aarseth, S. J., Pols, O. R., Eggleton, P. P., 1997, *MNRAS*, 291, 732